nature geoscience

SUPPLEMENTARY INFORMATION

DOI: 10.1038/NGEO843

Towards inferring earthquake patterns from geodetic observations of interseismic coupling

Nature Geoscience 2010

Yoshihiro Kaneko, Jean-Philippe Avouac, Nadia Lapusta

March 17, 2010

List of Tables

S1 The range of model parameters used to explore the correspondence between the non-dimensional parameter B and the model behavior (Fig. 4c,d). 13

List of Figures

S1 An example of shear stress evolution in the VS patch during coseismic slip. Shear stress τ with respect to a reference stress value $f_o\bar{\sigma}$ at the center of the VS patch (x = 120 km) is shown as a function of the coseismic slip of event 20 in Fig. 2b. The open circle indicates the stress τ_{vs}^{i} before the arrival of the dynamic rupture. The open triangle shows the peak shear stress τ_{vs}^{p}. The open square and the rectangle correspond to effective weakening distance d_{vs}^{c} and the amount of coseismic slip δ_{vs}, respectively. 14

S2 Additional simulation results illustrating how non-dimensional parameter B captures the behavior of the 2D model as its parameters are varied. (a-d) The dependence of the percentage P of two-segment ruptures on the properties of the VS patch as other model parameters are varied with respect to the simulations shown in Fig. 4a. In Fig. 4a, the following parameters are used: $\bar{\sigma}_{vw} = \bar{\sigma}_{vs} = 50$ MPa, $a_{vw} = 0.010$, $b_{vw} = 0.015$, and $D_{vw} = 72.5$ km. Panels (a-d) show results for a set of simulations with one or two of these parameters modified, as indicated at the top of each panel. The numbers in parentheses indicate the parameters in Fig. 4a. Comparison of panels (b-d) illustrates that the parameters of the VW segments also play an important role. (e) Relation between the percentage of two-segment ruptures P and the non-dimensional parameter B for cases in panels (a-d). The results collapse, with some scatter, onto a single curve. (f) Relation between P and B with (black dots) and without (purple dots) taking into account breakdown work in the estimate of B. Each dot corresponds to an earthquake sequence with different combination of model parameters as given by Table S1. 15

S3 A sketch illustrating the spring-slider system used to estimate ISC. The velocity-strengthening (VS) block in the middle represents the VS patch in the continuum models. The motion of the VS block is driven by the prescribed steady and stick-slip motions of the loading block and the VW block, respectively. 16

DOI: 10.1038/NGEO843

S4 Behavior of the velocity-strengthening (VS) block in the spring-slider model illustrated in Fig. S3. We assume that $k_{\rm vw} = \mu/D_{\rm vs}$ and $k_{\rm pl} = \mu/(R+D_{\rm vs})$ as discussed in the text and take $\mu = 30$ GPa, $V_{\rm pl} = 5$ cm/s, and $\sigma_{\rm vs} = 50$ MPa, the same values as for the continuum models. (a) Slip as a function of time for two earthquake cycles of the model, as given by Eq. (S26). (b-d) The dependence of interseismic coupling (ISC) given by Eq. (S34) on the interseismic period T, the rate-and-state parameter $a_{\rm vs} - b_{\rm vs}$, and the typical interaction distance R that determines the spring stiffness $k_{\rm pl}$ between the VS block and the loading block. 17

S1 Computation of Interseismic Coupling (ISC)

Interseismic coupling (ISC) is defined as the ratio of slip deficit during the interseismic period divided by the long term slip that would have happened if the fault had been slipping at it long term average slip rate. In our model, ISC at any location x on the fault is computed from $\mathrm{ISC}(x) = 1 - \delta_{\mathrm{int}}^{\mathrm{cum}}(x)/[V_{\mathrm{pl}} T_{\mathrm{int}}^{\mathrm{cum}}(x)]$, where $T_{\mathrm{int}}^{\mathrm{cum}}$ is sum of the interseismic time intervals at the location x for the entire simulation and $\delta_{\mathrm{int}}^{\mathrm{cum}}$ is the slip accumulated at x over all interseismic periods. The interseismic periods $T_{\mathrm{int}}(x)$ are defined to be the time when slip rate $V(x,t)$ is less than the long-term slip rate V_{pl}.

S2 Description of the fault models and parameters

We use fault models (*Lapusta et al.*, 2000; *Lapusta and Liu*, 2009) in which earthquakes are simulated as a part of spontaneously occurring earthquake sequences on a fault that is subjected to slow, tectonic-like loading. This approach allows us to study naturally developing earthquakes, with conditions before the nucleation originating from the previous history of fault slip rather than from arbitrarily selected prestress. Our simulations resolve all stages of the seismic cycle: the aseismic nucleation process in gradually varying zones of accelerating slip, the subsequent inertially controlled event (unstable slip) with realistic slip rates and rupture speeds, the postseismic slip, and the interseismic quasi-static deformation between events.

The fault is governed by rate and state friction with the aging form of state variable evolution. For situations with time-independent effective normal stress $\bar{\sigma}$, the shear strength τ is expressed as

$$\tau = \bar{\sigma}\left[f_0 + a\ln\left(\frac{V}{V_0}\right) + b\ln\left(\frac{V_0\theta}{L}\right)\right], \tag{S1}$$

$$\frac{d\theta}{dt} = 1 - \frac{V\theta}{L}, \tag{S2}$$

where a and b are rate and state constitutive parameters, V is slip rate, f_0 is the reference friction coefficient corresponding to the reference slip rate V_0, θ is a state variable which can be interpreted as the average age of the population of contacts between two surfaces, and L is the characteristic slip for state evolution (*Dieterich*, 1978, 1979; *Ruina*, 1983). The actual fault resistance to sliding in our model is given by rate and state friction regularized at zero slip velocity (*Lapusta et al.*, 2000). The response of constitutive laws (Eq. S1-S2), when extrapolated to coseismic slip rates, becomes qualitatively similar to the one given by linear slip-weakening friction (*Cocco and Bizzarri*, 2002) commonly used in dynamic rupture models (*Day et al.*, 2005).

We use parameters applicable to natural faults or derived from laboratory experiments except for characteristic slip L. The typical value of L used is 8 mm, larger than the laboratory values of the order of 1-100 μm, to make the breakdown work (sometimes called seismological fracture energy) comparable to values inferred from observational studies. For instance, the estimated breakdown work in the example in Fig. 2 is 2 MJ/m^2, which falls in the range of the breakdown work inferred for M>7 earthquakes (*Abercrombie and Rice*, 2005). Unless stated otherwise, we use the following set of parameters: $\mu = 30$ GPa, $c_s = 3.3$ km/s, $\bar{\sigma} = 50$ MPa, $f_0 = 0.6$, $V_0 = 10^{-6}$

DOI: 10.1038/NGEO843

m/s, $a_{\rm vw} = 0.010$, $b_{\rm vw} = 0.015$, and the size of the VW segment $D_{\rm vw} = 72.5$ km, where the subscript 'vw' is used to denote quantities related to the VW segments.

S2.1 Two-dimensional (2D) fault model

The 2D fault model is based on an antiplane (Mode III) framework in which purely dip-slip motion is assumed. Only along-strike (parallel to the x axis) variations are considered. The relation between slip $\delta(x,t)$, slip velocity $V(x,t) = \partial\delta(x,t)/\partial t$, and the corresponding shear stress $\tau(x,t)$ is given by (*Rice*, 1993; *Lapusta et al.*, 2000)

$$\tau(x,t) \;=\; \tau^o(x) + f(x,t) - \frac{\mu}{2c_s}V(x,t)\;, \tag{S3}$$

where μ is the shear modulus, c_s is the shear wave speed, τ^o is the loading stress that would act on the interface if it were constrained against any slip, and $f(x,t)$ is a linear functional of prior slip over the causality cone. The last term, known as radiation damping, is extracted from the functional $f(x,t)$ so that $f(x,t)$ can be evaluated without concern for singularities. The details of the elastodynamic solution and simulation methodology can be found elsewhere (*Lapusta et al.*, 2000).

The simulated fault domain is 480 km long. Slip evolution is computed, based on the assumed friction law, on the 240-km long central portion, and the prescribed slip rate $V_{\rm pl} = 5$ cm/year is imposed on the two 120-km long outer portions of the model (Fig. 1b). The spatial cell size Δx needs to be small enough to properly resolve both the aseismic nucleation process and the cohesive zone size during dynamic rupture propagation. In all of our simulations, the proper resolution of the cohesive-zone imposes a more stringent constraint on the spatial discretization. The ratio $\Lambda/\Delta x$ of the cohesive zone size Λ to the cell size $\Delta x = 29$ m needs to be 3 or larger for faults with rate and state friction (*Kaneko et al.*, 2008). The value of Λ in a typical scenario is ≈ 0.3 km and hence $\Lambda/\Delta x > 3$ in our simulations. The resulting ratio $h^*_{\rm RA}/\Delta x = 2\mu bL/[\pi(b-a)^2\bar{\sigma}\Delta x] = 63$, where $h^*_{\rm RA}$ is the estimate of the nucleation size for $a/b \gtrsim 0.5$ (*Rubin and Ampuero*, 2005), is then high enough to properly resolve the nucleation processes.

Time t is discretized into variable time steps. The minimum value of the time step is related to the time $\Delta t_{\rm cell} = \Delta x/c_s$ needed for the shear wave to propagate through one spatial cell; it is given by $0.5\Delta x/c_s = 0.044$ s. Such a small value of $\Delta t_{\rm min}$ is needed because slip in one time step must be comparable to or smaller than the characteristic slip L of the friction law to resolve the state-variable evolution. The largest time step allowed in all simulations is 0.2 years. A typical simulation with 5000 years of simulated slip history takes 5 days on a single 2.33-GHz core.

S2.2 Three-dimensional (3D) fault model

The 3D model formulation (*Lapusta and Liu*, 2009) is an extension of the 2D one. The major difference is that the 3D fault model allows for variations in the along-dip direction (Fig. 1c). The relation between slip $\delta_i(x,z,t)$, slip velocity $V_i(x,z,t)$, and the corresponding shear stress $\tau_{yi}(x,z,t) = \tau_i(x,z,t)$, $i = x,y,z$ on the fault plane $y = 0$ is expressed as

$$\tau_i(x,z;t) \;=\; \tau^o_i(x,z) + f_i(x,z;t) - \eta_i V_i(x,z;t)\;, \tag{S4}$$

where $\eta_x = \eta_z = \mu/(2c_s)$, $\eta_y = \mu c_p/(2c_s^2)$ and c_p is the dilatational wave speed. The details of the elastodynamic solution and simulation methodology for the model can be found elsewhere (*Lapusta and Liu*, 2009).

To facilitate comparison between the 2D and 3D simulations, we use the same set of parameters except for two parameters that are only defined in the 3D model: the dilatational wave speed c_p and the seismogenic width W (Fig. 1c). We assign $c_p = \sqrt{3}c_s$ and $W = D_{vw}/2 = 36.25$ km. The effective normal stress $\bar{\sigma}(z)$ linearly increases in the down-dip direction, from 30 MPa at the top of the simulated region to 70 MPa at the bottom of it, with $\bar{\sigma}(z) = 50$ MPa along a horizontal line at the mid-depth of the seismogenic zone.

The simulated fault domain is 300 km long along strike and 150 km wide along dip. The along strike-variations are the same as in the 2D models. In the along-dip direction, we consider a 75-km wide region, where slip is determined by solving the elastodynamic equations based on the assumed friction law, and two 37.5-km wide loading regions with prescribed slip rate (Fig. 1c). The cell size is $\Delta x = \Delta z = 0.14$ km, and the cohesive zone size Λ in a 3D simulation is ≈ 0.3 km. Hence, $\Lambda/\Delta x \approx 2.2$, which gives marginal but acceptable discretization (*Day et al.*, 2005; *Kaneko et al.*, 2008). Since a 3D simulation is much more computationally expensive than a 2D one, we performed a total of seven 3D simulations with different values of parameters $\bar{\sigma}_{vs}(a_{vs} - b_{vs})$ or D_{vs} (Fig. 4c,d). With the geometry and spatial discretization adopted here, a 3D simulation for an earthquake sequence that produces 30-40 events takes one week with 250 cores on a supercomputer.

S3 Construction of the non-dimensional model parameter B

To construct parameter B that determines the probability that seismic rupture would propagate through the VS patch, we consider the ratio of the following two quantities: (i) stress increase required for the patch to sustain seismic slip, and (ii) stress transferred from the ruptured VW segment to the VS patch.

Let us first consider the stress increase required for the VS patch to sustain seismic slip integrated over the patch, $C = \Delta\tau_{prop} D_{vs}$, where $\Delta\tau_{prop}$ is the average required amount of shear stress increase and D_{vs} is the size of the VS patch. We refer to C as the VS patch resistance. To estimate $\Delta\tau_{prop}$, let us first consider the difference in shear stress on the VS patch before and during seismic slip. Prior to the arrival of seismic rupture, the shear stress on the VS patch is given by:

$$\tau_{vs}^{i} = \bar{\sigma}_{vs}\left[f_0 + (a_{vs} - b_{vs}) \ln\left(V_{vs}^{i}/V_0\right)\right] , \tag{S5}$$

where V_{vs}^{i} is the representative interseismic slip rate in the VS patch. During seismic slip with slip rate V_{vs}^{dyn}, shear stress in the patch can be approximated as

$$\tau_{vs}^{d} = \bar{\sigma}_{vs}\left[f_0 + (a_{vs} - b_{vs}) \ln\left(V_{vs}^{dyn}/V_0\right)\right] . \tag{S6}$$

DOI: 10.1038/NGEO843

Hence

$$\Delta\tau_{\rm prop} = \tau_{\rm vs}^{\rm d} - \tau_{\rm vs}^{\rm i} = \bar{\sigma}_{\rm vs}(a_{\rm vs} - b_{\rm vs}) \ln\left(V_{\rm vs}^{\rm dyn}/V_{\rm vs}^{\rm i}\right) \ . \tag{S7}$$

This analysis ignores the larger but shorter-lived stress increase at the rupture tip, which becomes progressively more important as $(a_{\rm vs} - b_{\rm vs})$ approaches zero; a velocity-neutral patch would still provide resistance to the rupture propagation through the breakdown work at the rupture tip. This effect can actually be incorporated. At the onset of seismic slip with slip rate $V_{\rm vs}^{\rm dyn}$, the shear stress in the VS patch abruptly increases to a peak value approximately given by

$$\tau_{\rm vs}^{\rm p} = \bar{\sigma}_{\rm vs}\left[f_0 + a_{\rm vs}\ln\left(V_{\rm vs}^{\rm dyn}/V_0\right) + b_{\rm vs}\ln\left(V_0/V_{\rm vs}^{\rm i}\right)\right] \ , \tag{S8}$$

and drops to the value $\tau_{\rm vs}^{\rm d}$ given by Eq. (S6) over the effective weakening distance $d_{\rm vs}^{\rm c}$ (Fig. S1). The resulting breakdown work density is given by $(\tau_{\rm vs}^{\rm p} - \tau_{\rm vs}^{\rm d})d_{\rm vs}^{\rm c}/2$, and this part of work is additional to the friction work density $(\tau_{\rm vs}^{\rm d} - \tau_{\rm vs}^{\rm i})\delta_{\rm vs}$ that arises due to stress increase (Eq. S7), where $\delta_{\rm vs}$ is the amount of seismic slip averaged over the patch. Hence to account for the transient stress increase at the rupture tip, we write

$$\Delta\tau_{\rm prop} = \frac{d_{\rm vs}^{\rm c}}{2\delta_{\rm vs}}(\tau_{\rm vs}^{\rm p} - \tau_{\rm vs}^{\rm d}) + (\tau_{\rm vs}^{\rm d} - \tau_{\rm vs}^{\rm i}) \tag{S9}$$

$$= \bar{\sigma}_{\rm vs}(a_{\rm vs} - \lambda^* b_{\rm vs}) \ln\left(V_{\rm vs}^{\rm dyn}/V_{\rm vs}^{\rm i}\right) \ , \tag{S10}$$

where

$$\lambda^* \equiv 1 - d_{\rm vs}^{c}/(2\delta_{\rm vs}) \ . \tag{S11}$$

The patch resistance to seismic slip can therefore be written as:

$$C = \Delta\tau_{\rm prop} D_{\rm vs} = \bar{\sigma}_{\rm vs}(a_{\rm vs} - \lambda^* b_{\rm vs}) D_{\rm vs} \ln\left(V_{\rm vs}^{\rm dyn}/V_{\rm vs}^{\rm i}\right) \ . \tag{S12}$$

The first term on the right-hand side of Eq. (S9) corresponds to the contribution from the transient stress increase at the crack tip, and, in most cases we have considered, it amounts to a few percent of the second term. Let us estimate λ^*. For the rate and state friction with the aging form of state variable evolution, the effective weakening distance is given by (*Cocco and Bizzarri*, 2002; *Rubin and Ampuero*, 2005) $d_{\rm vs}^{\rm c} = L_{\rm vs}\ln(V_{\rm vs}^{\rm dyn}/V_{\rm vs}^{\rm i})$, where $\ln(V_{\rm vs}^{\rm dyn}/V_{\rm vs}^{\rm i}) \approx 20$ in our simulations, nearly independently of the properties of the VS patch as discussed in the main text. $\delta_{\rm vs}$ can be estimated as a fraction (we use 1/2) of the maximum slip in the nearby velocity-weakening segment. If $\Delta\tau_{\rm vw}$ is the average stress drop over the VW segment, $D_{\rm vw}$ is the size of the VW segment, and rupture over the VW segment is approximated as a quasi-static crack, then we have $\delta_{\rm vs} = \Delta\tau_{\rm vw} D_{\rm vw}/(2\mu)$. Hence we get

$$\lambda^* = 1 - \frac{\mu L_{\rm vs}\ln(V_{\rm dyn}/V_{\rm i})}{\Delta\tau_{\rm vw} D_{\rm vw}} \ . \tag{S13}$$

For the typical values of the model parameters, both assigned ($\mu = 30$ GPa, $L_{\rm vs} = 8$ mm, $D_{\rm vw} = 72.5$ km) and resulting in the model ($\Delta\tau_{\rm vw} = 3$ MPa, $\ln(V_{\rm vs}^{\rm dyn}/V_{\rm vs}^{\rm i}) \approx 20$), we obtain

$\lambda^* = 0.98$. This is why the effect represented by λ^* can be ignored for patches that are not close to velocity-neutral, with the patch resistance C approximately given by $C_{\rm appr}$ defined in the main text. Note that the smaller the characteristic slip $L_{\rm vs}$ of the rate and state friction, the closer the value of λ^* to one.

Now let us consider the stress transferred to the VS patch by rupture of a VW segment. We start from the 2D elastodynamic equation (Eq. S3), where shear stress distribution $\tau(x)$ during a seismic event can be written as

$$\tau(x) \;=\; \tau^{\rm before}(x) + f(x,t) - \frac{\mu}{2c_s} V(x) \;, \tag{S14}$$

where $\tau^{\rm before}(x)$ is shear stress before the event and $f(x,t)$ is redefined accordingly. Integrating Eq. (S14) over the entire fault after the rupture of a single VW segment, we obtain

$$\int_x \tau(x)dx \;=\; \int_x \tau^{\rm before}(x)dx - \frac{\mu}{2c_s}\int_x V(x)dx \;, \tag{S15}$$

since the integral over $f(x,t)$ is zero (*Zheng and Rice*, 1998). The last term on the right-hand side is negligible compared to others, since slip velocity after the end of a seismic event is small ($V \lesssim 1$ mm/s). Ignoring that term, we obtain

$$\int_x \left[\tau(x) - \tau^{\rm before}(x)\right] dx = 0 \;, \tag{S16}$$

or

$$\int_{\rm vw} \left[\tau(x) - \tau^{\rm before}(x)\right] dx + \int_{\rm vs} \left[\tau(x) - \tau^{\rm before}(x)\right] dx = 0 \;. \tag{S17}$$

Considering the situation where one of the VW segments has ruptured and transferred stress onto the surrounding VS regions, we get

$$\int_0^{D_{\rm vw}} \Delta\tau_{\rm vw}(x)dx \equiv \Delta\tau_{\rm vw} D_{\rm vw} = \int_{\rm VS\ patch} \Delta\tau_{\rm vs}(x)dx + \int_{\rm VS\ other} \Delta\tau_{\rm vs}(x)dx \;, \tag{S18}$$

where $\Delta\tau_{\rm vw}(x)$ and $\Delta\tau_{\rm vw}$ are the coseismic stress drop and its average value over the VW segment, respectively, and $\Delta\tau_{\rm vs}$ is the stress increase over the VS areas. Hence we can write

$$\int_{\rm VS\ patch} \Delta\tau_{\rm vs}(x)dx = \beta\Delta\tau_{\rm vw} D_{\rm vw} \;, \tag{S19}$$

where β is a model-dependent geometric factor that specifies the fraction of the stress transferred onto the VS patch (with the remainder being transferred onto the larger VS region adjacent to the ruptured VW segment). We use $\beta = 1/2$ for the 2D model and $\beta = W/(2W + 2D_{\rm vw}) = 1/6$ for the 3D model, respectively, by assuming that stress is transferred equally in all directions and that, in 3D, β is proportional to the perimeter of the VW segment that is contiguous with the VS patch.

We construct the non-dimensional parameter B as the ratio of the patch resistance (Eq. S12)

DOI: 10.1038/NGEO843

and representative stress increase provided by ruptures of VW segments (Eq. S19):

$$B = \frac{\Delta\tau_{\rm prop} D_{\rm vs} W}{\beta \Delta\tau_{\rm vw} D_{\rm vw} W} = \frac{\bar{\sigma}_{\rm vs}(a_{\rm vs} - \lambda^* b_{\rm vs}) D_{\rm vs} \ln(V_{\rm dyn}/V_{\rm i})}{\beta \Delta\tau_{\rm vw} D_{\rm vw}} , \tag{S20}$$

where λ^* is given by Eq. (S13). For the 3D model, the seismogenic fault width W would multiply both the numerator and denominator of Eq. (S20) and hence parameter B remains the same. In computing parameter B, we estimate $\Delta\tau_{\rm vw}$ for each simulation by taking the average stress drop within a VW segment of one-segment ruptures from that simulation and set $\ln(V_{\rm dyn}/V_{\rm i}) = 20$ for all cases. We would expect seismic events to preferentially propagate through the patch if B is small. For larger value of B, we expect a smaller percentage of earthquakes to propagate through the patch.

As discussed in the main text, parameter B is indeed correlated with the probability P that an event that has ruptured one of the VW segments would propagate through the VS patch. Fig. S2 illustrates this using a number of 2D simulation examples. Panels (a-d) show the effect of the characteristic velocity strengthening $\bar{\sigma}(a_{\rm vs} - b_{\rm vs})$ and of the size $D_{\rm vs}$ of the VS patch on the probability P for four different cases in which other parameters, including parameters of the VW segments, are varied. The properties of the VS patch have a systematic effect on P when other parameters are fixed, as discussed in the main text. Comparison of panels (b-d) shows that properties of the VW segments also have a significant effect. However, all these results collapse, with some scatter, onto a single curve when we compute parameter B for all simulation represented by dots in Fig. S2a-d and plot the resulting values of B against the percentage P of two-segment ruptures (Fig. S2e). If the contribution of the breakdown work at the crack tip is ignored, or equivalently if $\lambda^* = 1$ is assumed, then the correspondence between B and P for most values of B remains good, except for small values of B (Fig. S2f), consistent with our earlier estimate.

S4 Interseismic coupling (ISC) derived from a spring-slider model

Here we analyze the relationship between interseismic coupling (ISC) and the model parameters based on a simple spring-slider model, for the cases of the VS patch acting as a permanent barrier ($P = 0$). This analysis explains why ISC is relatively high even for such cases, as shown in Fig. 4d, and motivates the dependence of ISC on the parameter $B_{\rm appr}$ that also governs the seismic behavior of the model. The spring-slider model illustrated in Fig. S3 is a plausible simplification of our model in that slip within the central velocity-strengthening (VS) patch is driven by plate loading as well as by motion of the neighboring velocity-weakening (VW) segments.

We consider periodic model behavior, in which the VW block has earthquakes every T years, with (instantaneous) slip $V_{\rm pl}T$, and the VS block responds in the interseismic period with both postseismic and interseismic slip. The quasi-static equation for the shear stress τ acting on the central block that represents the VS patch is given by

$$\tau = \tau_{\rm i} - (\delta - \delta_{\rm vw})k_{\rm vw} - (\delta - V_{\rm pl}t)k_{\rm pl} , \tag{S21}$$

where $\tau_{\rm i}$ is the initial shear stress of the VS block, δ is the slip of the VS block, $\delta_{\rm vw}$ is the

prescribed motion of the VW block that represents a VW segment, t is time, $V_{\rm pl}t$ is the motion of the block that represents plate loading, and $k_{\rm vw}$ and $k_{\rm pl}$ are stiffnesses associated with the springs that connect the VS block to the VW block and the loading block, respectively. For comparison with the continuum models, the spring stiffnesses can be written in the form μ/D, where μ is the shear modulus and D is the typical spatial scale over which the elastic interaction occurs. For the interaction between the creeping VS patch and the locked VW segment, we take the characteristic spatial scale as $D_{\rm vs}$, since the locked region is adjacent to the VS patch. For the interaction between the creeping VS patch and the loading segments, the characteristic spatial scale is $(R + D_{\rm vs})$, where R is the distance between the VS patch and the fault areas that creep with the loading rate in our numerical models. Hence, we take:

$$k_{\rm vw} = \mu/D_{\rm vs} \ , \ k_{\rm pl} = \mu/(R + D_{\rm vs}) \ , \tag{S22}$$

where $R = D_{\rm vw}$ for the 2D model. For the 3D model, R is smaller, comparable to the seismogenic depth W.

Let $t = 0$ correspond to the end of one of the interseismic periods, so that one of the earthquakes experienced by the VW block occurs at $t = 0^+$. Then Eq. (S21) can be rewritten for $0^+ < t < T$ as

$$\tau = \tau_{\rm i} - \delta k_{\rm vw} - (\delta - V_{\rm pl}t)k_{\rm pl} + \Delta\tau_{\rm vs} \ , \tag{S23}$$

where $\Delta\tau_{\rm vs} = V_{\rm pl}Tk_{\rm vw}$ is the shear stress increase on the VS block due to the sudden slip of the VW block and $\delta(0^+) = \delta_{\rm i} = 0$.

The frictional strength $\tau_{\rm str}$ of the VS block is:

$$\tau_{\rm str} = \tau_{\rm i} + \bar{\sigma}_{\rm vs}(a_{\rm vs} - b_{\rm vs}) \ln(V/V_{\rm i}) \ , \tag{S24}$$

where $V_{\rm i}$ is the initial slip rate of the VS patch and it is assumed that the block remains in steady state throughout its motion as supported by our simulations. The equation of motion of the VS block is given by $\tau = \tau_{\rm str}$. The periodic behavior of the VS patch is enforced by requiring that

$$V(T) = V_{\rm i} \ , \tag{S25}$$

which leads to $\tau(T) = \tau_{\rm f}(T) = \tau_{\rm i}$ based on Eq. (S24) and $\delta(T) = V_{\rm pl}T$ based on Eq. (S21). Hence, in one period, all blocks in the model move by $V_{\rm pl}T$, as required for periodic behavior.

The mathematical form of a spring-slider problem similar to the one formulated here can be found elsewhere (*Perfettini and Avouac*, 2004). The resulting $\delta(t)$ and $V(t)$ are given by

$$\delta(t) = V_{\rm f}t_r \ln\left[1 + \Omega\frac{V_{\rm i}}{V_{\rm f}}(\exp(t/t_r) - 1)\right] \ , \tag{S26}$$

$$V(t) = V_{\rm i}\frac{\Omega\exp(t/t_r)}{1 + \Omega\frac{V_{\rm i}}{V_{\rm f}}\left[\exp(t/t_r) - 1\right]} \ , \tag{S27}$$

DOI: 10.1038/NGEO843

where

$$\Omega = \exp\left[\frac{\Delta\tau_{\rm vs}}{\bar{\sigma}_{\rm vs}(a_{\rm vs}-b_{\rm vs})}\right] , \tag{S28}$$

$$t_r = \frac{\bar{\sigma}_{\rm vs}(a_{\rm vs}-b_{\rm vs})}{V_{\rm pl}k_{\rm pl}} , \tag{S29}$$

$$V_{\rm f} = \frac{V_{\rm pl}k_{\rm pl}}{k_{\rm vw}+k_{\rm pl}} . \tag{S30}$$

From the periodic condition (Eq. S25), we obtain

$$V_{\rm i} = \frac{V_{\rm f}}{\Omega}\left(\frac{\Omega\exp(T/t_r)-1}{\exp(T/t_r)-1}\right) . \tag{S31}$$

Note that $V_{\rm f} < V_{\rm pl}$ since $k_{\rm vw} > 0$ and $k_{\rm pl} > 0$, and $V_{\rm f}$ gives the slip velocity of the VS block at which the stress changes on the VS block due to elastic interactions with the locked VW block and with the steadily moving loading block would exactly balance. Further, for $\Omega \gg 1$ and $T \gg t_r$ as typical for the range of parameters from the continuum models, $V_{\rm i} \approx V_{\rm f}$. The evolution of slip (Eq. S26) of the VS block predicts postseismic relaxation curves similar to those observed in the continuum models (Fig. 2f). An example of slip evolution given by Eq. (S26) for $\Omega = 100$ and $T/t_r = 6$ is plotted in Fig. S4a.

Let us now compute ISC of the VS block, which is determined by the slip deficit accumulated over the period when the VS block slides with slip velocity less than $V_{\rm pl}$. Setting $V(t_{\rm Vpl}) = V_{\rm pl}$, where $t_{\rm Vpl}$ is the time at which the VS block slows down to $V_{\rm pl}$ (Fig. S4a), solving for $t_{\rm Vpl}$, and finding the slip at time $t = t_{\rm Vpl}$, we get:

$$\delta(t_{\rm Vpl}) = V_{\rm f}t_r \ln\left[\frac{V_{\rm f}(\Omega-1)}{(1-\exp(-T/t_r))(V_{\rm pl}-V_{\rm f})}\right] . \tag{S32}$$

The total slip in one period is given by

$$\delta(T) \equiv V_{\rm pl}T = V_{\rm f}t_r\left(\ln\Omega + T/t_r\right) . \tag{S33}$$

Hence

$$\mathrm{ISC} = \frac{\delta(t_{\rm Vpl})}{\delta(T)} = \frac{\ln(\Omega-1) - \ln[1-\exp(-T/t_r)] - \ln\left[(V_{\rm pl}-V_{\rm f})/V_{\rm f}\right]}{\ln\Omega + T/t_r} . \tag{S34}$$

We plot the ISC predicted by the spring-slider model for a range of the sizes $D_{\rm vs}$ of the VS patch, periods T observed in the 2D simulations, and the rate and state parameters $(a_{\rm vs}-b_{\rm vs})$ (Fig. S4b,c). The values of ISC shown in (Fig. S4b,c) are comparable to the ones obtained in the continuum simulations with $P = 0$ (Fig. 4b,d). In particular, the ISC is relatively high, larger than 0.6 for most parameter combinations, just as observed in the continuum simulations. In addition, Eq. (S34) predicts that ISC is lower for smaller R (Fig. S4d), consistent with the lower values of the ISC found in the 3D simulations compared to those in the 2D simulations (Fig. 4d). In the 3D model, the larger VS region adjacent to the top and bottom of the VS patch would act as a loading region, so that $R \approx W < D_{\rm vw}$, leading to the lower values of ISC.

Let us simplify Eq. (S34) assuming the parameter regime motivated by the 2D continuum model, with $\Omega \gg 1$, $T \gg t_r$, and $R = D_{\rm vw} \gg D_{\rm vs}$. Then ISC is given by

$$\mathrm{ISC} = 1 - \frac{\bar{\sigma}_{\rm vs}(a_{\rm vs} - b_{\rm vs})D_{\rm vs}}{V_{\rm pl}T\mu} \ln\left(\frac{D_{\rm vw}}{D_{\rm vs}}\right) . \tag{S35}$$

Let us further assume that the coseismic slip of a VW segment is related to its average stress drop $\Delta\tau_{\rm vw}$ through a quasi-static crack model, so that $V_{\rm pl}T = D_{\rm vw}\Delta\tau_{\rm vw}/\mu$. Then

$$\mathrm{ISC} = 1 - \frac{\bar{\sigma}_{\rm vs}(a_{\rm vs} - b_{\rm vs})D_{\rm vs}}{\Delta\tau_{\rm vw}D_{\rm vw}} \ln\left(\frac{D_{\rm vw}}{D_{\rm vs}}\right) . \tag{S36}$$

Eq. (S36) shows that ISC primarily depends on the quantity $F = \bar{\sigma}_{\rm vs}(a_{\rm vs} - b_{\rm vs})D_{\rm vs}/(\Delta\tau_{\rm vw}D_{\rm vw})$. This quantity also appears in the approximate expression $B_{\rm appr}$ for the non-dimensional parameter B that governs the seismic behavior of the continuum models. In fact, F and $B_{\rm appr}$ differ only by the geometric model-dependent parameter β which obviously cannot be captured by a spring-slider model. Hence this analysis motivates the dependence of ISC on B discussed in the main text.

DOI: 10.1038/NGEO843

References

Abercrombie, R. E., and J. R. Rice, Can observations of earthquake scaling constrain slip weakening?, *Geophys. J. Int.*, *162(2)*, 406–424, 2005.

Cocco, M., and A. Bizzarri, On the slip-weakening behavior of rate and state dependent constitutive laws, *Geophys. Res. Lett.*, *29(11)*, 2002.

Day, S. M., L. A. Dalguer, N. Lapusta, and Y. Liu, Comparison of finite difference and boundary integral solutions to three-dimensional spontaneous rupture, *J. Geophys. Res.*, *110*, 2005.

Dieterich, J. H., Time-dependent friction and the mechanics of stick-slip, *J. Geophys. Res.*, *116*, 790–806, 1978.

Dieterich, J. H., Modeling of rock friction: 1. Experimental results and constitutive equations, *J. Geophys. Res.*, *84*, 2,161–2,168, 1979.

Kaneko, Y., N. Lapusta, and J.-P. Ampuero, Spectral element modeling of spontaneous earthquake rupture on rate and state faults: Effect of velocity-strengthening friction at shallow depths, *J. Geophys. Res.*, *113*, 2008.

Lapusta, N., and Y. Liu, Three-dimensional boundary integral modeling of spontaneous earthquake sequences and aseismic slip, *J. Geophys. Res.*, 2009.

Lapusta, N., J. Rice, Y. Ben-Zion, and G. Zheng, Elastodynamic analysis for slow tectonic loading with spontaneous rupture episodes on faults with rate- and state-dependent friction, *J. Geophys. Res.*, *105*, 23,765–23,789, 2000.

Perfettini, H., and J. P. Avouac, Postseismic relaxation driven by brittle creep: A possible mechanism to reconcile geodetic measurements and the decay rate of aftershocks, applications to the Chi-Chi earthquake, Taiwan, *J. Geophys. Res.*, *109*, 2004.

Rice, J. R., Spatio-temporal complexity of slip on a fault, *J. Geophys. Res.*, *98*, 9,885–9,907, 1993.

Rubin, A. M., and J.-P. Ampuero, Earthquake nucleation on (aging) rate and state faults, *J. Geophys. Res.*, *110*, 2005.

Ruina, A. L., Slip instability and state variable friction laws, *J. Geophys. Res.*, *88*, 10,359–10,370, 1983.

Zheng, G., and J. R. Rice, Conditions under which velocity-weakening friction allows a self-healing versus a cracklike mode of rupture, *Bull. Seismol. Soc. Am.*, *88*, 1,466–1,483, 1998.

Table S1: The range of model parameters used to explore the correspondence between the non-dimensional parameter B and the model behavior (Fig. 4c,d).

Parameter	Symbol	2D model	3D model
Shear modulus	μ	30, 60 GPa	30 GPa
Characteristic slip distance in VW	L_{vw}	8, 16, 24 mm	8 mm
Characteristic slip distance in VS	L_{vs}	4, 8, 16, 24 mm	8 mm
Effective normal stress in VW	$\bar{\sigma}_{\mathrm{vw}}$	25, 50 MPa	50 MPa (mid-depth)
Effective normal stress in VS	$\bar{\sigma}_{\mathrm{vs}}$	25, 50 MPa	50 MPa (mid-depth)
The size of the VW segment	D_{vw}	$30-100$ km	72.5 km
The size of the VS patch	D_{vs}	$5-50$ km	$5, 10, 15$ km
Rate and state parameter a in VW	a_{vw}	$0.005-0.025$	0.01
Rate and state parameter a in VS	a_{vs}	$0.01-0.02$	0.01
Rate and state parameter b in VW	b_{vw}	$0.005-0.030$	0.015
Rate and state parameter b in VS	b_{vs}	$0-0.020$	$0.005, 0.007, 0.009$
Seismogenic width	W	N/A	36.25 km

DOI: 10.1038/NGEO843

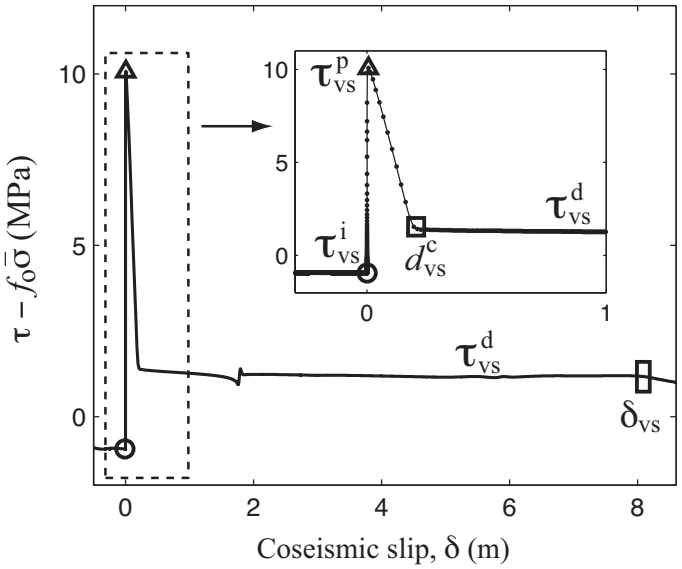

Figure S1: An example of shear stress evolution in the VS patch during coseismic slip. Shear stress τ with respect to a reference stress value $f_o\bar{\sigma}$ at the center of the VS patch ($x = 120$ km) is shown as a function of the coseismic slip of event 20 in Fig. 2b. The open circle indicates the stress τ^i_{vs} before the arrival of the dynamic rupture. The open triangle shows the peak shear stress τ^p_{vs}. The open square and the rectangle correspond to effective weakening distance d^c_{vs} and the amount of coseismic slip δ_{vs}, respectively.

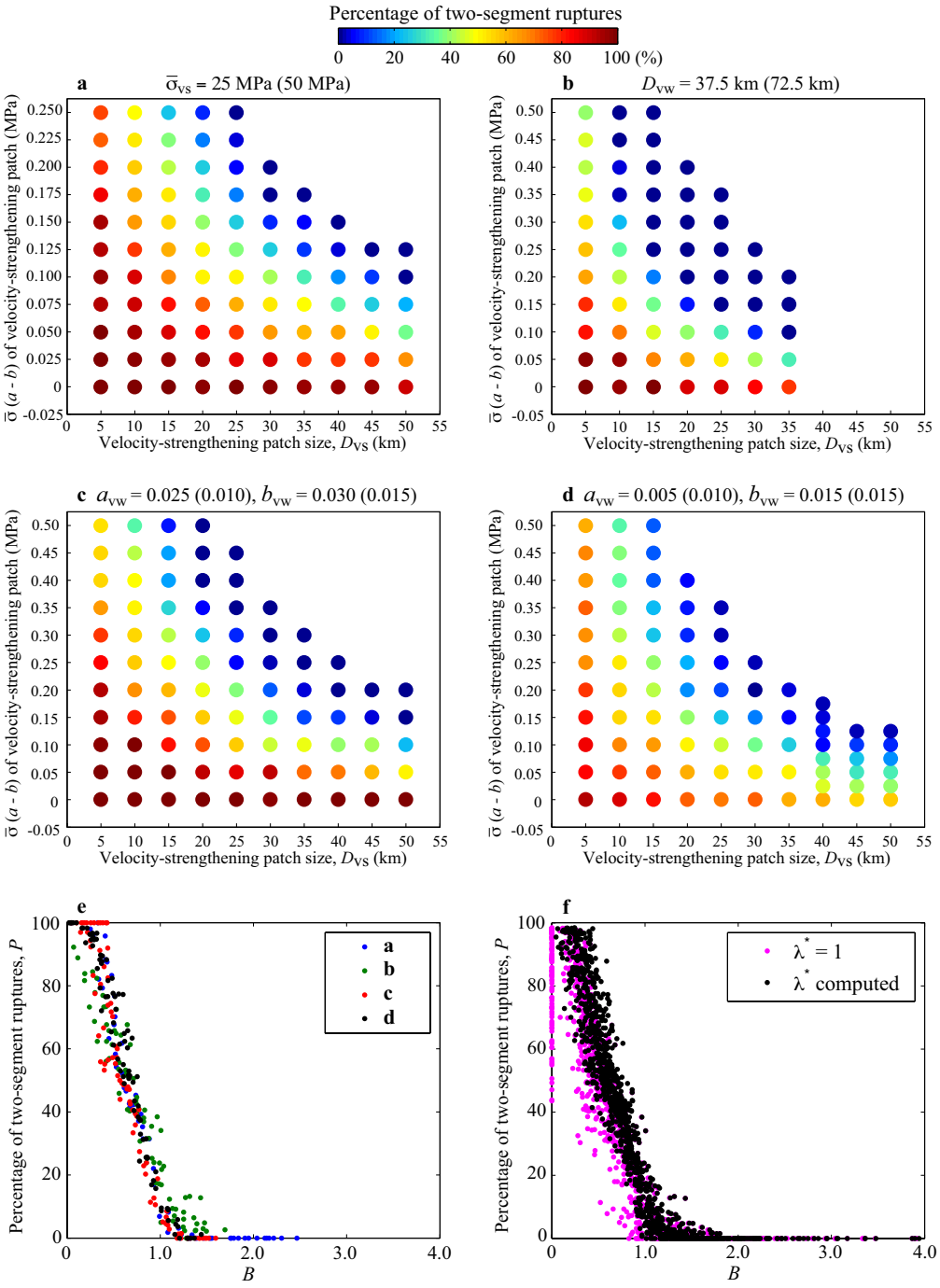

Figure S2: Additional simulation results illustrating how non-dimensional parameter B captures the behavior of the 2D model as its parameters are varied. (a-d) The dependence of the percentage P of two-segment ruptures on the properties of the VS patch as other model parameters are varied with respect to the simulations shown in Fig. 4a. In Fig. 4a, the following parameters are used: $\bar{\sigma}_{vw} = \bar{\sigma}_{vs} = 50$ MPa, $a_{vw} = 0.010$, $b_{vw} = 0.015$, and $D_{vw} = 72.5$ km. Panels (a-d) show results for a set of simulations with one or two of these parameters modified, as indicated at the top of each panel. The numbers in parentheses indicate the parameters in Fig. 4a. Comparison of panels (b-d) illustrates that the parameters of the VW segments also play an important role. (e) Relation between the percentage of two-segment ruptures P and the non-dimensional parameter B for cases in panels (a-d). The results collapse, with some scatter, onto a single curve. (f) Relation between P and B with (black dots) and without (purple dots) taking into account breakdown work in the estimate of B. Each dot corresponds to an earthquake sequence with different combination of model parameters as given by Table S1.

DOI: 10.1038/NGEO843

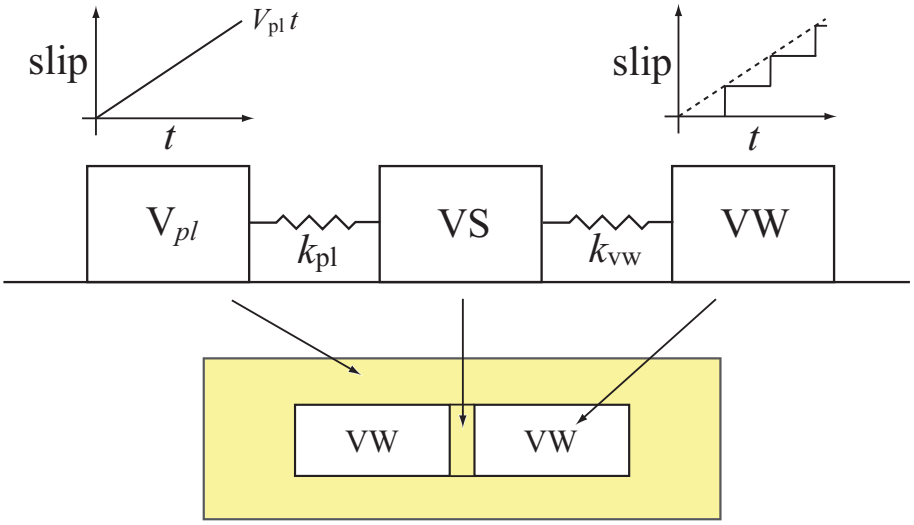

Figure S3: A sketch illustrating the spring-slider system used to estimate ISC. The velocity-strengthening (VS) block in the middle represents the VS patch in the continuum models. The motion of the VS block is driven by the prescribed steady and stick-slip motions of the loading block and the VW block, respectively.

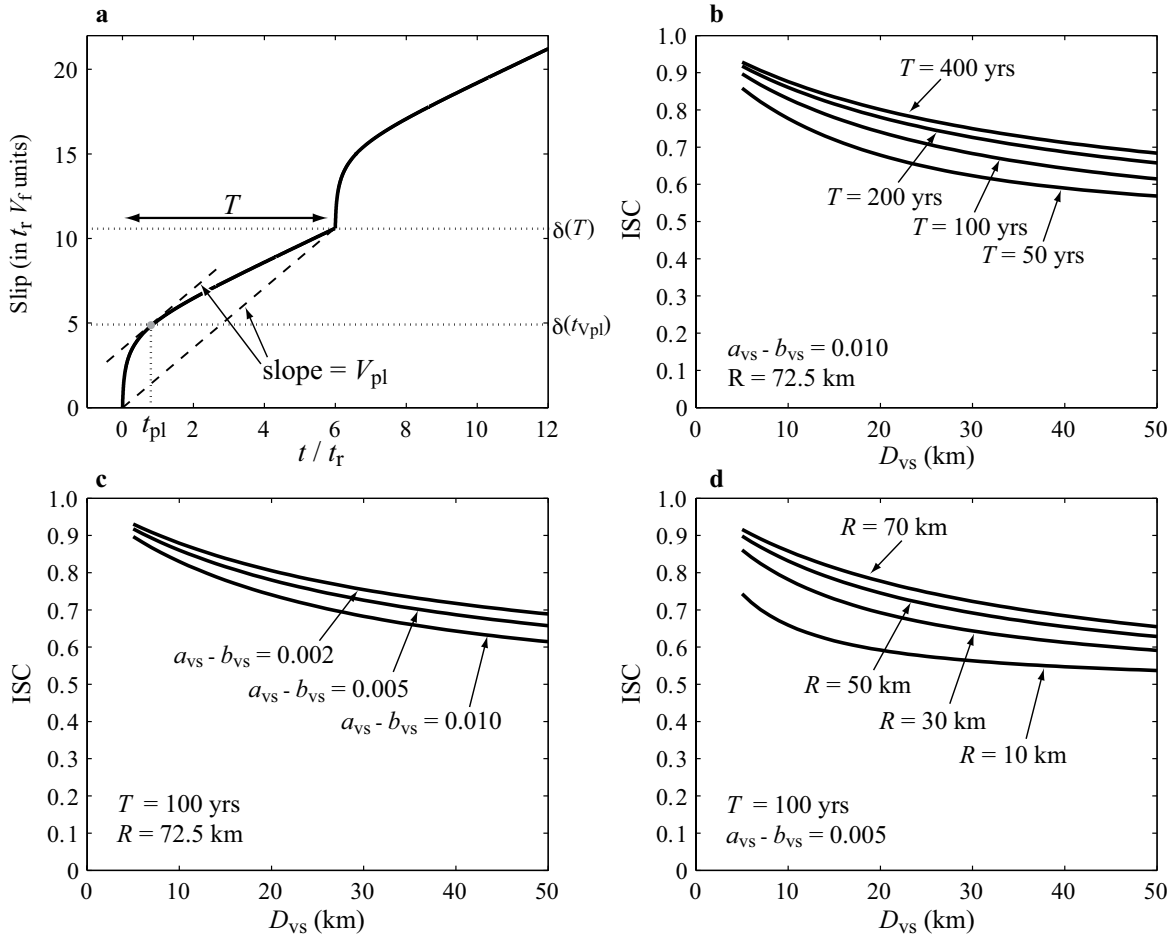

Figure S4: Behavior of the velocity-strengthening (VS) block in the spring-slider model illustrated in Fig. S3. We assume that $k_{vw} = \mu/D_{vs}$ and $k_{pl} = \mu/(R+D_{vs})$ as discussed in the text and take $\mu = 30$ GPa, $V_{pl} = 5$ cm/s, and $\sigma_{vs} = 50$ MPa, the same values as for the continuum models. (a) Slip as a function of time for two earthquake cycles of the model, as given by Eq. (S26). (b-d) The dependence of interseismic coupling (ISC) given by Eq. (S34) on the interseismic period T, the rate-and-state parameter $a_{vs} - b_{vs}$, and the typical interaction distance R that determines the spring stiffness k_{pl} between the VS block and the loading block.

DOI: 10.1038/NGEO843

Online Supplementary Movie for

Towards inferring earthquake patterns from geodetic observations of interseismic coupling

Nature Geoscience 2010

Yoshihiro Kaneko, Jean-Philippe Avouac, Nadia Lapusta

March 17, 2010

Movie S1: 3D simulation example of long-term fault behavior due to interaction of two seismogenic velocity-weakening (VW) segments separated by a velocity-strengthening (VS) patch. The VS patch creates complexity of large events in the model, acting as an occasional barrier to seismic rupture and causing clustering of large events. The VW segments and VS patch are surrounded by a larger VS region; the boundaries between areas of different friction properties are shown as white lines. The simulated time t is shown at the top in years. Colors represent slip rate on the fault, with seismic slip rates shown in white and bright yellow, postseismic slip and interseismic creep shown in orange and red, and locked portions shown in black. The interframe rate of the movie is variable, from several years in the interseismic period to several seconds during dynamic rupture propagation. The potency deficit is defined as $V_{\rm pl}tA - \int_A \delta dA$, where $V_{\rm pl}$ is the plate rate, δ is the accumulated slip, and A is the area of the region -92 km $\leq X \leq 92$ km and -25 km $\leq Z \leq 25$ km. The 6th simulated earthquake starts shortly after $t = 200$ years and ruptures both VW segments and the central VS patch. After the earthquake, the VS fault areas experience postseismic slip. In the interseismic period, the two VW segments are locked and the surrounding VS region is creeping. The creep is slowly penetrating into the locked regions due to stress concentrations between the creeping and locked areas. At $t = 229$ years, the 7-th event starts at the same location as the 6-th one but arrests at the VS patch. The resulting postseismic slip triggers the smaller 8-th and 9-th earthquakes about 9 and 10 days later, respectively. This leads to a complex pattern of smaller seismic events and aseismic transients in the right VW segment between $t = 230$ and $t = 266$ years. The potency deficit shows that the model is neither time-predictable nor slip-predictable. In the interseismic periods, the VS patch has slip rates of the order of 3×10^{-10} m/s, lower than the plate rate of 5 cm/yr $= 1.6 \times 10^{-9}$ m/s and corresponding to interseismic coupling of 0.80.